

Journal Pre-proof

Magnetocaloric effect in ErNi₂ melt-spun ribbons

J.L. Sánchez Llamazares, P. Ibarra-Gaytán, C.F. Sánchez-Valdés, D. Ríos-Jara, P. Álvarez-Alonso



PII: S1002-0721(19)30252-2

DOI: <https://doi.org/10.1016/j.jre.2019.07.011>

Reference: JRE 574

To appear in: *Journal of Rare Earths*

Received Date: 28 March 2019

Revised Date: 23 July 2019

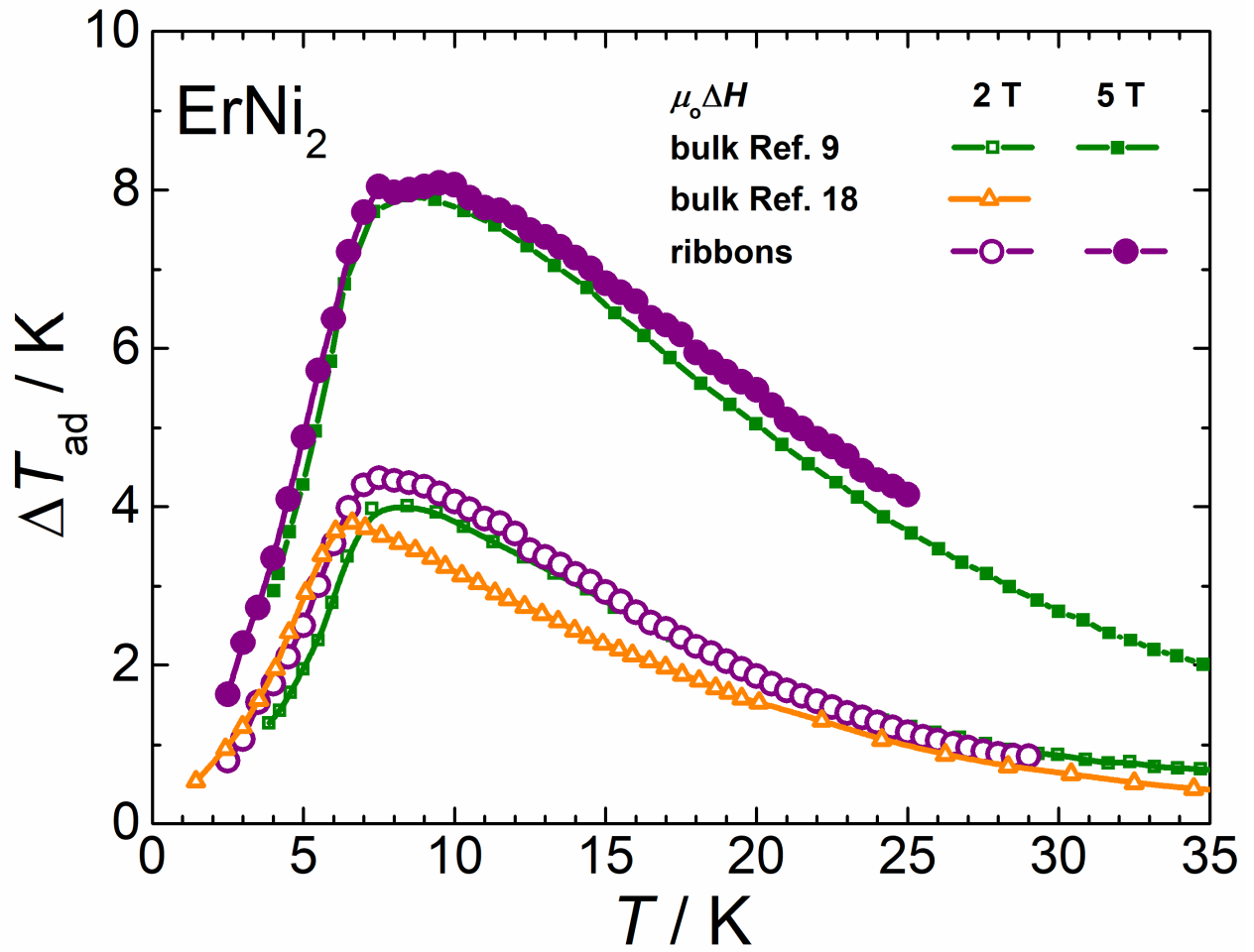
Accepted Date: 26 July 2019

Please cite this article as: Llamazares JLS, Ibarra-Gaytán P, Sánchez-Valdés CF, Ríos-Jara D, Álvarez-Alonso P, Magnetocaloric effect in ErNi₂ melt-spun ribbons, *Journal of Rare Earths*, <https://doi.org/10.1016/j.jre.2019.07.011>.

This is a PDF file of an article that has undergone enhancements after acceptance, such as the addition of a cover page and metadata, and formatting for readability, but it is not yet the definitive version of record. This version will undergo additional copyediting, typesetting and review before it is published in its final form, but we are providing this version to give early visibility of the article. Please note that, during the production process, errors may be discovered which could affect the content, and all legal disclaimers that apply to the journal pertain.

© [Copyright year] Published by Elsevier B.V. on behalf of Chinese Society of Rare Earths.

As-solidified isotropic melt-spun ribbons of the ErNi_2 Laves phase show excellent magnetocaloric properties.



Magnetocaloric effect in ErNi₂ melt-spun ribbons

J.L. Sánchez Llamazares,^{a,*} P. Ibarra-Gaytán,^{a,b} C.F. Sánchez-Valdés,^{c,**}
D. Ríos-Jara,^a P. Álvarez-Alonso^d

^a Instituto Potosino de Investigación Científica y Tecnológica A.C., Camino a la Presa San José 2055, Col. Lomas 4^a, San Luis Potosí, S.L.P. 78216, México.

^b CPM-TIP, University Pavol Jozef Safárik, Park Angelinum 9, 04154 Kosice, Slovakia.

^c División Multidisciplinaria, Ciudad Universitaria, Universidad Autónoma de Ciudad Juárez (UACJ), calle José de Jesús Macías Delgado # 18100, Ciudad Juárez 32579, Chihuahua, México.

^d Departamento de Física, Universidad de Oviedo, Calvo Sotelo s/n, 33007 Oviedo, Spain.

ErNi₂ ribbons were produced by rapid solidification using the melt spinning technique. Their structural, magnetic and magnetocaloric properties in the as-solidified state were studied by X-ray diffraction, scanning electron microscopy, magnetization and specific heat measurements. Samples are single phase with the MgCu₂-type crystal structure, a Curie temperature T_C of 6.8 K and a saturation magnetization at 2 K and 5 T of 124.0 A·m²/kg. For a magnetic field change $\mu_0\Delta H$ of 5 T (2 T) ribbons show a maximum magnetic entropy change $|\Delta S_M^{\text{peak}}|$ of 24.1 (16.9) J/(kg·K), and an adiabatic temperature change $\Delta T_{\text{ad}}^{\text{max}}$ of 8.1 (4.4) K; this is similar to the previously reported literature for bulk alloys that were processed through conventional melting techniques followed by prolonged thermal annealing. In addition, the samples also show slightly wider $\Delta S_M(T)$ curves with respect to bulk alloys leading to a larger refrigerant capacity.

Keywords: ErNi₂ Laves phase; melt-spun ribbons; magnetic entropy change; adiabatic temperature change.

Foundation item: Project supported by the SEP-CONACYT, Mexico (grant number A1□S□37066); the MINECO, Spain (grant number MAT2014-56116-C4-R); and Principado de Asturias, Spain (grant number IDI/2018/000185).

* **Corresponding author:** Prof. J.L. Sánchez Llamazares (**E-mail:** jose.sanchez@ipicyt.edu.mx; **Tel.:** +52-444-8342000).

** **Corresponding author:** Dr. C.F. Sánchez-Valdés (**E-mail:** csanchez@nanomagnetics.org; **Tel.:** +52-656-6882100).

1. Introduction

In the past three decades, the magnetocaloric properties of a long list of rare-earth metals, their solid solutions and rare-earth-based intermetallic compounds have been studied.¹⁻⁶ Rare-earth (RE) intermetallic compounds based on heavy rare earths elements undergoing a second-order ferromagnetic-to-paramagnetic transition are of particular interest because they might show a large reversible magnetocaloric effect (MCE) in the temperature range of nitrogen and hydrogen liquefaction (i.e., from 10 to 80 K). In these compounds, the high magnetic moment of the lanthanide leads to a high saturation magnetization M_S , whereas the crystalline field at the RE site may lead to a sui-generis anisotropic behaviour of magnetization. Among them, binary ferromagnetic Laves phases RNi_2 with $R = Tb, Dy, Ho,$ or Er , have received significant attention since they are stable, easy to produce and below 50 K exhibit large maximum magnetic entropy $|\Delta S_M^{\text{peak}}|$ and adiabatic temperature $\Delta T_{\text{ad}}^{\text{max}}$ changes.⁷⁻⁹ In view of that, they have been referred as suitable working substances for their use in cryogenic magnetic refrigerators.^{10,11}

These compounds typically crystallize into the cubic $MgCu_2$ -type crystal structure with the space group $Fd\bar{3}m$ (also known as the C15 structure of Laves phases),¹² and their magnetism only comes from the large localized magnetic moment of the 4f rare earth element (i.e., Ni atoms do not carry a magnetic moment) and their parallel coupling through the exchange interaction via conduction electrons. Present contribution reports the magnetocaloric (MC) properties of as-solidified melt-spun ribbons of the intermetallic compound $ErNi_2$ with the available data of literature reported for bulk alloys. This compound shows the lowest Curie temperature (T_C) among the above-mentioned ones (around 7 K),¹³⁻¹⁵ as well as an interesting anisotropic behaviour of magnetization as revealed by *D. Gignoux* and *F. Givord*,¹⁶ who performed magnetization measurements at 1.5 K up to a high magnetic field of 14 T for a single crystal through the significant crystallographic directions. Their study demonstrated that the spontaneous magnetization at $\mu_0 H = 0$ is found throughout the [100] direction although the crystalline field favours the [111] direction. The spontaneous magnetization through those directions were $5.0 \mu_B/Er^{+3}$ and $2.9 \mu_B/Er^{+3}$, respectively. Furthermore, along both the [111] and [110] crystalline directions, the magnetization $M(\mu_0 H)$ increases rapidly at relatively low fields, surpassing the magnetization obtained along the [100] direction; the differences become significant above 2 T, since the magnetization along the easy direction tends to saturate, whereas along [110] and [111] directions progressively rise with the increasing of the magnetic field.

The existing information on the magnetocaloric properties of $ErNi_2$ is limited to the theoretical earlier calculations done by *von Ranke et al.*⁸ and then by *Plaza et al.*⁹, and the experimental studies carried out by *Tomokiyo et al.*¹⁷ and more recently by *Ćwik et al.*¹⁸ The study of *Plaza et al.* considered the conventional and anisotropic magnetocaloric effect;⁹ for the conventional MCE they compared the shape and trend that were obtained for the $\Delta S_M(T)$ and $\Delta T_{\text{ad}}(T)$ curves that were in reasonable agreement with the experimental data. Their calculations were based on a Hamiltonian that considered the effects of the crystalline electrical field, the exchange interaction in a molecular-field approximation, and the Zeeman energy; the authors highlighted that the results of this theoretical calculation are more accurate than in their previous work.⁸ To the best of our knowledge, all the experimental results reported on the magnetocaloric properties of this compound correspond to bulk polycrystalline alloys that were produced by arc melting followed by a long-term thermal annealing under vacuum at temperatures

between 1100 and 1173 K from 2 to 20 days.^{9,17,18} The present research was undertaken to fabricate ErNi₂ melt-spun ribbons in order to assess their MC response. This fabrication technique has been successfully applied in recent years to synthesize the isostructural Laves phases RNi₂ with R = Tb, Dy, Ho).¹⁹⁻²¹

2. Experimental procedure

First, a 4 gram ingot with the stoichiometric composition ErNi₂ was produced by Ar arc-melting from highly pure Er (99.9 %, Sigma Aldrich) and Ni (99.998 %, Alfa Aesar). To ensure its good starting homogeneity, the ingot was re-melted three times; the final mass of the as-cast ingot coincided with the starting one. From this sample, melt-spun ribbons flakes were obtained under a highly pure Ar atmosphere at a linear speed of the rotating copper wheel of 25 m/s in an Edmund Bühler model SC melt spinner system.

The X-ray diffraction (XRD) pattern of finely powdered melt-spun ribbons was recorded between 20° and 100° with a 2 θ increment of 0.01° in a high-resolution Rigaku Smartlab diffractometer with a wavelength of 0.15418 nm corresponding to Cu-K α radiation. A dual beam scanning electron microscope (SEM), Helios Nanolab model ESEM FEI Quanta 200, was used in order to obtain secondary electron images of the microstructure; the system was equipped with an energy dispersive spectroscopy (EDS) detector.

The magnetic measurements were carried out using a 9 Tesla Quantum Design Dynacool[®] Physical Property Measurement System (PPMS) by means of the vibrating sample magnetometer option. Measurements were done on a needed-like ribbon sample applying the external magnetic field through the major length ribbon axis (that it is coincident with the rolling direction) to reduce the effect of the internal demagnetizing field. The temperature dependence of the specific magnetization, the $M(T)$ curves, were measured under static magnetic fields of 5 mT and 5 T at a temperature sweeping rate of 1.0 K/min. The specific heat c_p as a function of temperature was measured by using the heat capacity module of a Quantum Design Evercool-I[®] PPMS[®] system; this option measures the thermal response of a small thin sample by means of a thermal-relaxation calorimeter.

3. Results and discussion

Figure 1(a) shows several representative secondary electron SEM images of the ribbons microstructure. The foreground image corresponds to the free surface, whereas the cross-section appears at the inset. Ribbons are polycrystalline, they show an average ribbon thickness of 21 μm , and are composed by micrometers in size grains with no visible orientation with respect to the ribbon plane. The cross-section shows a homogeneous distribution of grains, with no appreciable differences in grain morphology, in contrast to the columnar growth trend that has been observed in other RNi₂ melt-spun ribbons.^{20,21} No secondary phases are observed. A large number of EDS analyses, performed on both ribbon surfaces and their cleaved cross-section, confirmed the average 1:2 composition in the fabricated samples (within a 0.1 at. % of instrumental error). Figure 1(b) displays the room temperature X-ray powder diffraction pattern together with the Le Bail refinement performed using the FullProf suite package.²² It was correctly indexed considering the Bragg reflections of the cubic MgCu₂-type crystal structure of the Laves phases (Strukturbericht designation: C15; space group: Fd $\bar{3}$ m; PDF card: 04-001-

0543); the cubic structure shows a lattice constant $a = 0.7126(1)$ nm. No evidence of secondary phases, either amorphous or crystalline, was found in the pattern (which agrees with SEM observations). As Table 1 evidences, the determined lattice constant is in good agreement with the values found in literature for bulk alloys.^{13,18,23,24} Selecting several flat ribbons, a second XRD pattern was recorded (not shown) by directing the X-ray beam onto their free surface. No significant differences were found in the intensities of the Bragg reflections of this XRD pattern with respect to the one displayed in Figure 1(b), confirming the absence of meaningful crystallographic texture. It is well known that ribbons fabrication by melt spinning of metallic crystalline alloys is a quite empirical process and the attainment of grain-oriented ribbons of a given material is not a simple task. With such a purpose, the effect of several synthesis parameters, such as linear speed of the copper wheel, temperature of the molten alloy (that strongly influences its viscosity), nozzle-to-wheel distance, ejection angle, and overpressure to eject the liquid, on ribbons' microstructure must be carefully studied and favorably combined.

Temperature dependencies of magnetization at low- and high-magnetic fields are presented in Figure 1(c). The low magnetic field curve unveils that the material undergoes a single well-defined second-order magnetic phase transition. From the minimum of the first derivative of the $M(T)$ plot at 5 mT (displayed in the inset) in the phase transition region we obtained a Curie temperature T_C of 6.8 K. As Table 1 shows, this is in good agreement with the available data for bulk ErNi_2 alloys. The effective magnetic moment μ_{eff} estimated from the Curie-Weiss law was $9.61 \mu_B$, which is slightly below the recently reported by *Ćwik et al.* of $9.8 \mu_B$.¹⁸ The $M(T)$ curve at 5 T spreads out over a wide temperature interval across the magnetic transition region; the observed shift of its inflexion point towards a temperature higher than T_C is explained by the interaction of the magnetic moments with the strong applied magnetic field that tends to keep the ferromagnetic order. Samples show a saturation magnetization M_S at 2 K and 5 T of $124.0 \text{ A}\cdot\text{m}^2/\text{kg}$ which is lower by about 7.4 % than the early value reported by *Voiron*²⁵ and close to the reported by *Ćwik et al.* ($\sim 126 \text{ A}\cdot\text{m}^2/\text{kg}$)¹⁸ for bulk alloys.

In order to characterize the MC response of the ribbon samples, we measured a set of isothermal magnetization curves up to $\mu_0 H_{\text{max}} = 5$ T (with a temperature step of 0.5 K between consecutive curves), as well as the temperature dependence of the specific heat $c_p(T)$ at zero magnetic field; the resulting curves appear in Figures 2(a) and (b), respectively. $M(\mu_0 H)$ isotherms illustrate that ribbons do not reach the saturated state even at $\mu_0 H = 5$ T, in agreement with the observed behavior of both single-crystal and polycrystalline ErNi_2 .^{16,18} Roughly speaking, the shape and values of the $c_p(T)$ dependence are consistent with those previously reported;^{13-15,17,18} the curve exhibits the typical λ -type shape at the ferromagnetic-paramagnetic phase transition. From $c_p(T)$ we calculated the thermal dependence of the total entropy at zero field as $S_T(T) = \int_0^T \frac{c_p(T')}{T'} dT'$ (also plotted in Figure 2(b)). Figure 3(a) shows the $\Delta S_M(T)$ curves for magnetic field changes $\mu_0 \Delta H$ of 2 and 5 T obtained from numerical integration of the Maxwell relation (i.e., $\Delta S_M(T, \mu_0 \Delta H) = \mu_0 \int_0^{\mu_0 H_{\text{max}}} \left[\frac{\partial M(T, \mu_0 H')}{\partial T} \right]_{\mu_0 H'} dH'$), whereas the relevant MC parameters derived from these curves are listed in Table 2. From $S_T(T)$ and the $\Delta S_M(T)$ curves obtained from Maxwell relation, we determined $S_T(T, \mu_0 \Delta H) = S_T(T, 0) + \Delta S_M(T, \mu_0 \Delta H)$ (not shown) and estimated the $\Delta T_{\text{ad}}(T)$ curves for $\mu_0 \Delta H = 2$ and 5 T from $\Delta T_{\text{ad}}(T_0, \mu_0 \Delta H) = T(S_T, \mu_0 H) - T(S_T, 0) = T(S_T, \mu_0 H) - T_0$;²⁶ the results are plotted in Figure 3(b). In Figures 3(a) and (b) we compared the $\Delta S_M(T)$ and $\Delta T_{\text{ad}}(T)$ curves for magnetic field changes of 2 and 5 T with the experimental^{9,17,18} and theoretical⁹ data informed

in literature. Note that, as it was expected, the maximum for both $|\Delta S_M(T)|$ and $\Delta T_{ad}(T)$ curves appears at $T \sim T_C$. ΔT_{ad}^{\max} reaches values of 4.4 and 8.1 K at 2 and 5 T, respectively. For a more comprehensive comparison, the significant parameters are listed in Table 2. It is also worth mentioning that these values agree, within the expected uncertainty, with those of bulk polycrystalline alloys. This situation coincides to the previously found for as-solidified TbNi₂ ribbons,¹⁹ and contrasts with the behavior of DyNi₂²⁰ and HoNi₂²¹ ribbons, in which enhanced MC properties were obtained due to the favorable combination of texture effects along ribbon length (extrinsic feature) and the anisotropic behavior of magnetization (i.e., due to the angle between the magnetic field and easy magnetization direction). But it is consistent with the absence of preferential grain growth in the fabricated ribbon samples. In order to verify the isotropic nature of the ribbons, a powdered sample was prepared from several ribbon flakes. The powder was carefully mixed with a tiny amount of GE-7031 varnish into a cylindrical in shape VSM powder sample holder. The sample was sonicated during several minutes in order to disperse particles until varnish solidification; this procedure avoids any preferential orientation of powder particles upon the application of an external magnetic field (i.e., preserving their spatial random orientation). The MC properties of this sample, that has been referred to as “pulverized ribbons”, derived from the $\Delta S_M(T)$ curves at 2 and 5 T are listed in Table 2. Notice that $|\Delta S_M^{\text{peak}}|$ value for melt-spun and pulverized ribbons for both magnetic field changes do not show a significant difference, highlighting the isotropic behavior of the MCE in the ErNi₂ melt-spun ribbons.

We have also determined the refrigerant capacity (*RC*), a figure of merit typically used to compare the amount of heat that can be removed from the load and to the environment by the working substance during an ideal refrigeration cycle. The *RC* is commonly estimated through three methods (hereafter referred to as *RC-1*, *RC-2*, and *RC-3*): *RC-1* = $|\Delta S_M^{\text{peak}}| \times (T_{\text{hot}} - T_{\text{cold}})$, *RC-2* = $\int_{T_{\text{cold}}}^{T_{\text{hot}}} |\Delta S_M(T)| dT$ (T_{hot} and T_{cold} are the temperatures that define the temperature interval δT_{FWHM} of the full width at half-maximum of the $|\Delta S_M(T)|$ curve: $\delta T_{\text{FWHM}} = T_{\text{hot}} - T_{\text{cold}}$), and *RC-3* as the maximum rectangular area that can be inscribed below the $|\Delta S_M(T)|$ curve.²⁶⁻²⁸ Relevant data of the ErNi₂ ribbons for 2 and 5 T have been gathered in Table 2; note that the as-quenched and pulverized ribbons display comparable *RC*'s for $\mu_0 \Delta H = 5$ T as a result of their similar $\Delta S_M(T)$ curves. When comparing them to the estimated parameters from the reported $\Delta S_M(T)$ in the literature (see Table 2), one can observe certain dispersion of values; nevertheless, those obtained from the ribbons are slightly larger mainly due to their extended span temperatures.

4. Conclusions

To conclude, we have evidenced that through the melt-spinning technique we were able to produce monophasic melt-spun ribbons of the ErNi₂ Laves phase with similar structural, magnetic, and magnetocaloric properties than the reported for bulk polycrystalline alloys that were fabricated using the conventional arc-melting technique followed by long-term high-temperature thermal annealing. The absence of texture explains the isotropic magnetocaloric response of the fabricated ribbon samples along the longitudinal direction; however, the slight extension of the working temperature span in comparison with the reported for bulk alloys leads to a moderate, but perceptible improvement of their refrigerant capacity.

Acknowledgements

The support received from the following organizations is gratefully acknowledged: (a) Laboratorio Nacional de Nanociencias y Nanotecnología (LINAN, IPICYT); (b) Consejo Potosino de Ciencia y Tecnología (COPOCYT), and; (c) Banco Santander Central Hispano and University of Oviedo. Authors are also indebted to M.Sc. B.A. Rivera-Escoto, M.Sc. A.I. Peña Maldonado and Dr. G.J. Labrada-Delgado for the technical support given. P.J. Ibarra Gaytán thanks to CONACYT for supporting his doctoral and postdoctoral studies at IPICYT and UPJS, respectively. C.F. Sánchez-Valdés is grateful to DMCU-UACJ for supporting his research stays at IPICYT (program PFCE and academic mobility grant); also, for the financial support received from SEP-CONACYT, Mexico. P. Alvarez-Alonso acknowledges the support received from MINECO, and Principado de Asturias, Spain.

References

1. Tishin AM. Magnetocaloric in the vicinity of phase transitions. In: Buschow KHJ, ed. Handbook of Magnetic Materials. Amsterdam: Elsevier. 1999;12:395.
2. Franco V, Blázquez JS, Ipus JJ, Law JY, Moreno-Ramírez LM, Conde A. Magnetocaloric effect: from materials research to refrigeration devices. *Prog Mater Sci.* 2018;93:112.
3. Zhang H, Gimaev R, Kovalev B, Kamilov K, Zverev V, Tishin A. Review on the materials and devices for magnetic refrigeration in the temperature range of nitrogen and hydrogen liquefaction. *Phys B: Cond Matter.* 2019;558:65.
4. Li LW. Review of magnetic properties and magnetocaloric effect in the intermetallic compounds of rare earth with low boiling point metals. *Chinese Phys B.* 2016;25:037502.
5. Guo D, Li H, Zhang Y. Magnetic Phase transition and magnetocaloric effect in ternary $\text{Er}_2\text{Ni}_2\text{Ga}$ compound. *IEEE Trans Magn.* 2019;55:2500204.
6. Zhang Y. Review of the structural, magnetic and magnetocaloric properties in ternary rare earth $\text{RE}_2\text{T}_2\text{X}$ type intermetallic compounds. *J Alloys Compd.* 2019;787:1173.
7. de Oliveira NA, von Ranke PJ. Theoretical aspects of the magnetocaloric effect. *Rep Prog Rep.* 2010;489:89.
8. von Ranke PJ, Nóbrega EP, de Oliveira IG, Gomes AM, Sarthour RS. Influence of the crystalline electrical field on the magnetocaloric effect in the series RNi_2 (R= Pr, Nd, Gd, Tb, Ho, Er). *Phys Rev B.* 2001;63:184406.
9. Plaza EJR, de Sousa VSR, Reis MS, von Ranke PJ. A comparative study of the magnetocaloric effect in RNi_2 (R = Dy, Ho, Er) intermetallic compounds. *J Alloys Compd.* 2010;505:357.
10. Gschneidner Jr KA, Pecharsky VK, Tsokol AO. Recent development in magnetocaloric materials. *Rep Prog Phys.* 2005; 68:1479.
11. Jeong S, AMR (Active Magnetic Regenerative) refrigeration for low temperature. *Cryogenics.* 2014;62:193.
12. Buschow KHJ. Intermetallic compounds of rare-earth and 3d transition metals. *Rep Prog Phys.* 1977;40:1179.
13. Li R, Ogawa M, Hashimoto T. Magnetic intermetallic compound for cryogenic regenerator. *Cryogenics.* 1990;30:521.
14. Melero JJ, Burriel R, Ibarra MR. Magnetic interactions in Laves phases. Heat capacity of PrNi_2 , GdNi_2 and ErNi_2 . *J Magn Magn Mater.* 1995;140-144:841.
15. Gailloux M. The low temperature properties of $(\text{Dy}_{1-x}\text{Er}_x)\text{Ni}_2$ alloys. MS thesis. Iowa: Ames Laboratory, Iowa State University; 1994.
16. Gignoux D, Givord F. Quadrupolar interactions in ErNi_2 . *J Magn Magn Mater.* 1983;31-34:217.
17. Tomokiyo A, Yayama H, Wakabayashi W, Kuzuhara T, Hashimoto T, Sahashi M, et al. Specific heat and entropy of RNi_2 (R: rare earth heavy metals) in magnetic field. *Adv Engin Cryo.* 1986;32:295.
18. Ćwik J, Koshkid'ko Y, Nenkov K, Tereshina EA, Rogacki K. Structural, magnetic and magnetocaloric properties of HoNi_2 and ErNi_2 compounds ordered at low temperatures. *J Alloys Compd.* 2018;735:1088.
19. Sánchez Llamazares JL, Sánchez-Valdés CF, Ibarra-Gaytán PJ, Álvarez-Alonso P, Gorria P, Blanco JA. Magnetic entropy change and refrigerant capacity of rapidly solidified TbNi_2 alloy ribbons. *J Appl Phys.* 2013;113:17A912.

20. Ibarra-Gaytán P, Sánchez-Valdés CF, Sánchez Llamazares JL, Álvarez-Alonso P, Gorria P, Blanco JA. Texture-induced enhancement of the magnetocaloric response in melt-spun DyNi₂ ribbons. *Appl Phys Lett*. 2013;103:152401.
21. Sánchez Llamazares JL, Ibarra-Gaytán PJ, Sánchez-Valdés CF, Álvarez-Alonso P, Varga R. Enhanced magnetocaloric effect in rapidly solidified HoNi₂ melt-spun ribbons. *J Alloys Comp*. 2019;774:700.
22. Rodriguez Carvajal J. Recent advances in magnetic structure determination by neutron powder diffraction. *Physica B*. 1993;192:55.
23. Myakush O, Verbovytsky Y, Kotur B. Hydrogenation properties of alloys based on ErNi₂ binary compound. *J Phys Conf Series*. 2007;79:012018.
24. Jin T, Li C, Tang K, Chen L. Hydrogenation induced change in structures, magnetic properties and specific heats of magnetic regenerative material ErNi and ErNi₂. *Mater Trans*. 2013;54:363.
25. Voiron MJ. Aimantation sous champ fort de quelques composés, type phases de Laves, entre des métaux de transition et des terres rares. *C R Acad Sc Paris*. 1972;274:589.
26. Dinesen AR, Linderøth S, Mørup S. Direct and indirect measurement of the magnetocaloric effect in La_{0.67}Ca_{0.33-x}Sr_xMnO_{3±δ}. *J Phys Condens Matter*. 2005;17:6257.
27. Tishin AM, Spichkin YI. The magnetocaloric effect and its applications. Bristol: Institute of Physics Publishing, 2003.
28. Gschneidner Jr KA, Pecharsky VK, Pecharsky AO, Zimm CB. Recent developments in magnetic refrigeration. *Mater Sci Forum*. 1999;69:315.
29. Wood ME, Potter WH. General analysis of magnetic refrigeration and its optimization using a new concept: maximization of refrigerant capacity. *Cryogenics*. 1985;25:667.

FIGURE CAPTIONS

Figure 1. (a) SEM micrographs showing the ribbon free surface (foreground image) and cross-section (inset). (b) Experimental and Le Bail refinement (Bragg R-factor of 0.692) of the room temperature X-ray power diffraction of melt-spun ribbons. (c) Temperature dependence of the specific magnetization determined under low (5 mT; full red symbols) and high (5 T; full black symbols) magnetic fields. Inset: $dM/dT(T)$ curve at 5 mT; the Curie phase transition temperature T_C appears at 6.8 K.

Figure 2. (a) Magnetization isotherms determined from 2 to 30 K up to a maximum magnetic field of 5 T. (b) Specific heat c_p and total entropy S_T as a function of temperature measured in absence of magnetic field.

Figure 3. $\Delta S_M(T)$ (a) and $\Delta T_{ad}(T)$ (b) curves at $\mu_0\Delta H = 2$ and 5 T for as-solidified melt-spun ribbons compared with the available experimental and theoretical data reported in the literature.

TABLE CAPTIONS

Table 1. Lattice constant, Curie phase transition temperature and saturation magnetization at 2 K and 5 T for ErNi_2 melt-spun ribbons. The data are compared with the data reported for bulk alloys.

Table 2. ΔT_{ad}^{\max} , $|\Delta S_M^{\text{peak}}|$, refrigerant capacity determined following different criteria (i.e., $RC-1$, $RC-2$, and $RC-3$, see text for definition), and $\Delta S_M(T)$ full-width at half-maximum temperature parameters (at $\mu_0\Delta H = 2$ T and 5 T) for as-solidified ErNi_2 melt-spun ribbons compared with the obtained for pulverized ribbons, and calculated,⁹ and experimental data reported for bulk polycrystalline alloys.^{9,17,18}

TABLES

Table 1.

Alloy	a (nm)	T_c (K)	M_S^{5T} ($A \cdot m^2/kg$)
ErNi ₂ ribbons	0.7126(1) ^a	6.8 ^a	124 at 2.0 K ^a
ErNi ₂ bulk alloys	0.7123 ¹³ , 0.7117 ¹⁸ , 0.71249(4) ²³ , 0.7126 ²⁴	6.7 ¹³ , 6.5 ¹⁴ , 7 ¹⁶ , 6.5 ¹⁸ , 6.5 ²⁴	134 at 4.2 K ²⁵

^a This work.

Table 2.

Method	Magnetization measurements						Specific heat measurements						Theoretical calculation ^{9, a}	
	Melt-spun ribbons		Pulverized ribbons		Bulk ^{18, a}		Bulk ^{17, a, d}		Bulk ^{18, a, e}		Bulk ^{9, a, f}			
Samples state	2	5	2	5	2	5	2	4.86	2	5	2	5	2	5
$\mu_0 \Delta H$ (T)	2	5	2	5	2	5	2	4.86	2	5	2	5	2	5
ΔT_{ad}^{max} (K)	4.4 ^c	8.1 ^c	-	-	-	-	-	8.8	3.8	-	4.0	7.9	7.7	12.9
$/\Delta S_M^{peak}/$ (J/(kg·K))	14.1	20.0	12.4	20.2	15.1	24.3	-	24.1	13.4	-	13.5	20.3	18.2	27.2
RC-1 (J/kg)	146	382	118	347	88	314	-	375	123	-	120	330	160	373
RC-2 (J/kg)	113	299	91	274	63	229	-	291	94	-	91	257	118	273
δT_{FWHM} (K)	10.5	19.1	9.5	17	5.8	12.9	-	15.5	9.2	-	8.9	16.2	8.8	13.7
T_{hot} (K)	14.7	23.5	13.9	21.5	10.5	17.5	-	20.0	13.5	-	13.6	20.9	12.2	16.8
T_{cold} (K)	4.3	4.4	4.4	4.4	4.7	4.6	-	4.5	4.3	-	4.7	4.7	3.4	3.1
RC-3 (J/kg)	74	191	59	177	47	157	-	188	62	-	61	165	80	195
δT^{RC-3} (K)	10	18	10	16	8.4	13	-	15	10.5	-	10.2	16.1	9.5	19.8
T_{hot}^{RC-3} (K) ^b	14.5	22.5	14.3	20.4	13	17.4	-	19.5	14.5	-	14.6	20.8	12.6	22.4
T_{cold}^{RC-3} (K) ^b	4.4	4.5	4.3	4.7	4.4	4.6	-	4.6	4.0	-	4.4	4.7	3.1	2.6

^a Estimated values from the reported curves.^b Related to RC-3.^c Determined combining specific heat and entropy change curves determined from magnetization measurements.^d Annealed at 1173 K during 2 days in vacuum.^e Annealed at 1100 K during 1 month in vacuum.^f This work does not describe synthesis conditions.

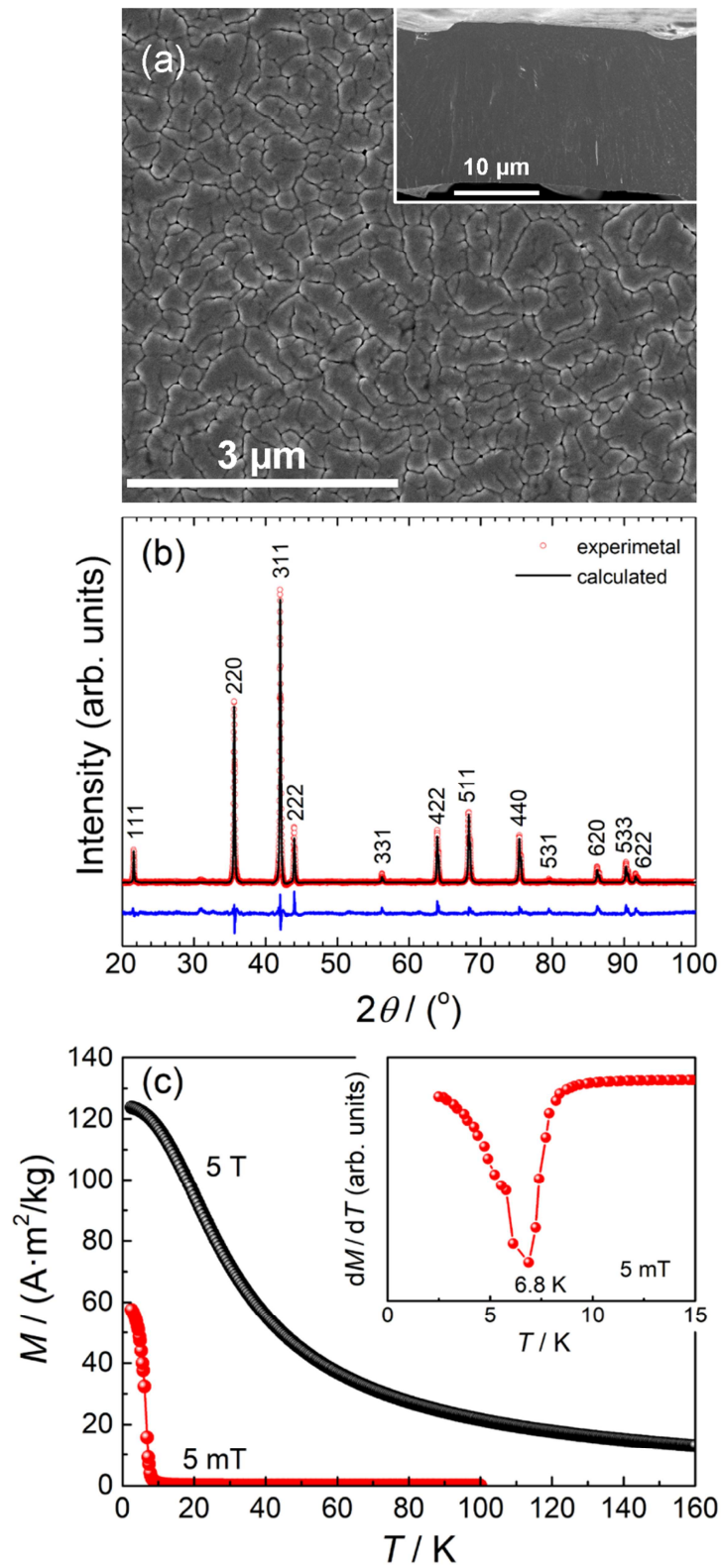


Figure 1.

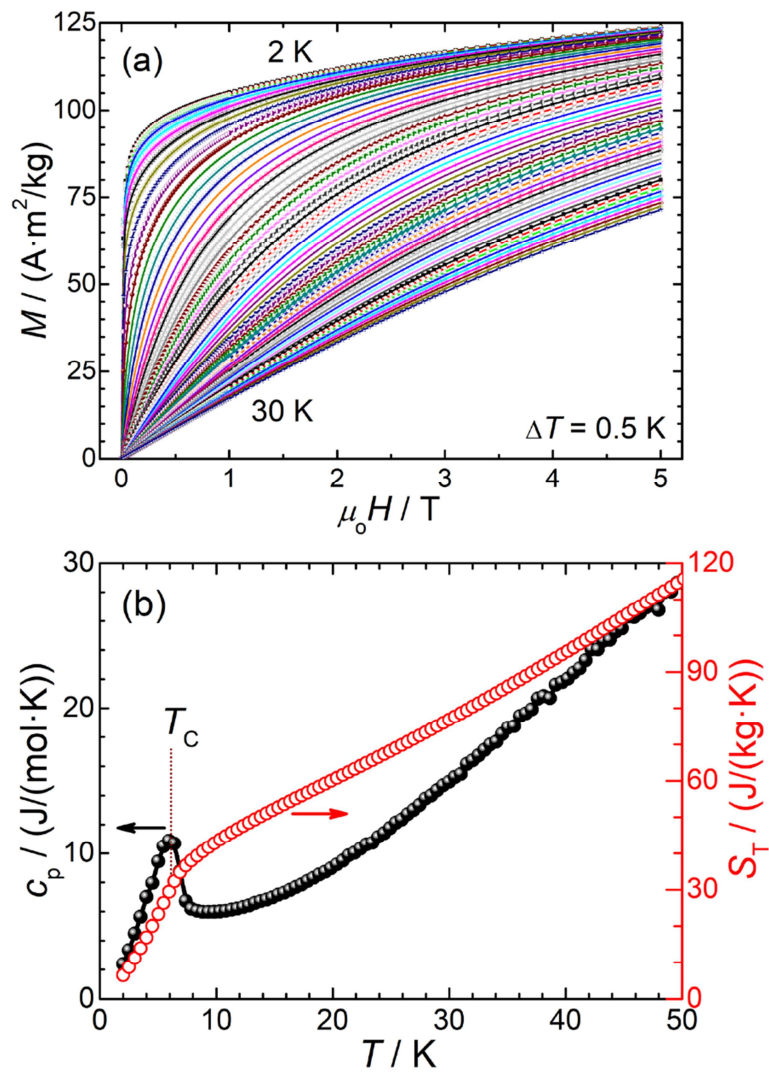


Figure 2.

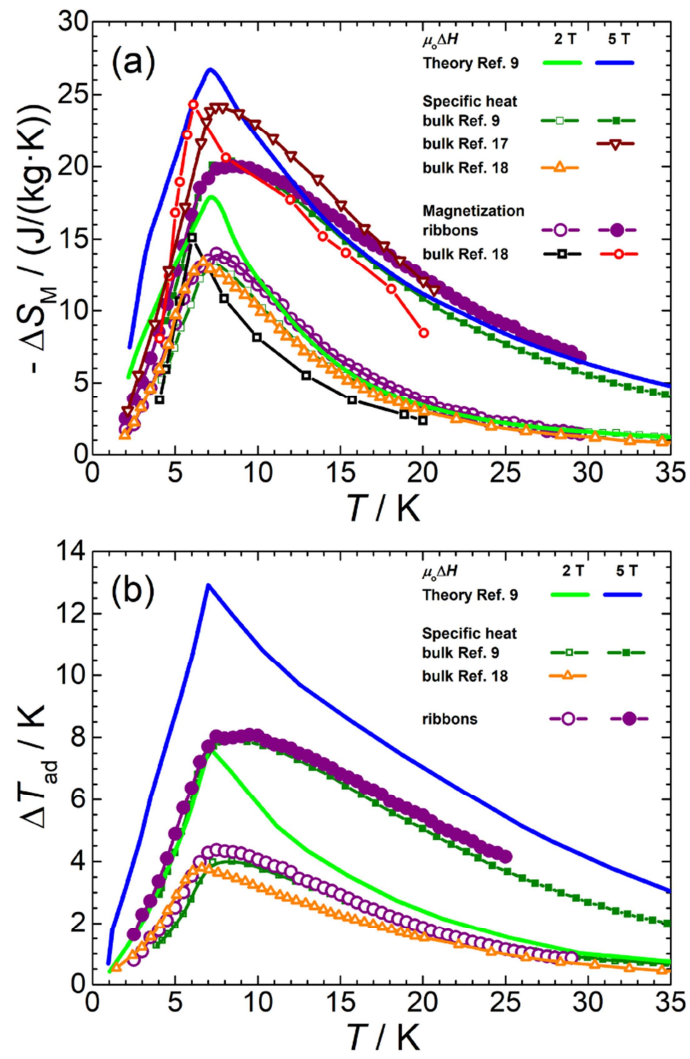


Figure 3.